Spectral functions of strongly correlated extended systems via an exact quantum embedding

George H. Booth* and Garnet Kin-Lic Chan
Department of Chemistry, Frick Laboratory, Princeton University, Princeton, New Jersey 08544, USA
(Dated: August 29, 2013)

Density matrix embedding theory (DMET) [PRL **109** 186404 (2012)], introduced the mapping of strongly correlated problems to the quantum embedding of an impurity with a finite set of bath states designed to exactly reproduce the entanglement of the ground state. The formalism provided similar physics to dynamical mean-field theory at a tiny fraction of the cost, but was limited the ground state properties. Here, we generalize the concept of quantum embedding to dynamic properties and demonstrate accurate bulk spectral functions at small computational cost. The proposed spectral DMET utilizes the Schmidt decomposition of a response vector, mapping the bulk dynamic correlation functions to that of a quantum impurity cluster coupled to a set of frequency dependent bath states. The resultant spectral functions are obtained on the real-frequency axis, without bath discretization error, from the solution of the resultant finite quantum impurity model. The formalism allows for arbitrary perturbations and correlation functions. We demonstrate the method on the 1D and 2D Hubbard model, where we obtain accurate zero temperature, thermodynamic limit spectral functions, and show the trivial extension to two-particle Greens functions. This advance vastly extends the scope and applicability of DMET in condensed matter problems as a computationally tractable route to correlated spectral functions of extended systems, and provides a competitive alternative to dynamical mean-field theory for dynamic quantities.

Dynamic correlation functions are directly probed in spectroscopic methods, and describe the transport, optical, magnetic and wider electronic structure properties of materials. As such, their accurate computation is highly sought after. However, few robust approaches exist for strongly correlated materials[1]. The difficulty is in simultaneously requiring both an accurate treatment of the electron correlations beyond mean-field density functional or low-order perturbation theory for the ground state *and* excitation spectrum, as well as modeling a system of sufficient size to reach the thermodynamic limit and not suffer spurious finite size effects. In general, only mean-field electronic structure methods are computationally cheap enough to access the required system sizes, and so there is a pressing need for methods with mean-field computational scaling, which can correctly describe the excitation spectrum in strongly correlated materials.

A zero-temperature dynamic correlation function can be defined in the frequency domain as

$$G(\omega;\hat{X},\hat{V}) = \langle\Psi^{(0)}|\hat{X}^\dagger \frac{1}{\omega-(H-E_0)+i\eta}\hat{V}|\Psi^{(0)}\rangle, \quad (1)$$

with the one- and two-particle Greens functions defined with $\hat{V}$ and $\hat{X}$ being single annihilation/creation or pairs of such operators respectively, with appropriate time-ordering of the operators. Spectral functions are defined as $A(\omega) = -\frac{1}{\pi}\Im[G(\omega)]$, where the spectral broadening is given by the small imaginary component of the energy, η, which regularizes the correlation function. The single particle density of states is the spectral function of the one-particle Greens function, experimentally measured by STM and (angle-resolved) photoemission spectroscopy. Two-particle spectral functions are also highly sought after, such as the two-hole propagator probed with Auger spectroscopy[2], or the particle-hole Greens function that gives the optical conductivity, polarizability and magnetizability, and are key descriptors in Raman spectroscopy and in the mechanism of high-T_c superconductivity[3–5].

One method which has proved useful in obtaining strongly correlated spectral functions is dynamical mean-field theory (DMFT)[6–8]. In DMFT, a single unit cell (or site) in the bulk is viewed as a quantum impurity, described by its local, one-particle Greens function, and is self-consistently embedded in a non-interacting Greens function (hybridization) from its environment. The quantum impurity problem, which is then solved via an 'impurity solver', such as continuous-time quantum Monte Carlo (CT-QMC)[9] or exact diagonalization (ED)[10]. However, there are some formal drawbacks of the DMFT formulation. The essential problem is that DMFT maps the infinite bulk onto a quantum impurity plus infinite bath problem, which is not much easier to solve. If CT-QMC is used as an impurity solver to integrate over this infinite bath (or indeed general QMC methods used in isolation), then spectral functions are obtained only on the imaginary frequency axis, requiring unstable analytic continuation onto the real frequency axis, which can wash out subtle or sharp features of the spectra[11]. Accessing low temperatures or arbitrary interactions produces Fermion sign problems, which can require millions of computer-hours to stabilize, even for a modest number of impurity sites. Exact diagonalization suffers from bath discretization error in the spectra due to the fitting of the hybridization (at all frequencies) to a small number of frequency independent bath sites. In addition, since DMFT is formulated using the one-particle Greens function, other spectra such as the two-particle Greens function and optical spectra are difficult to obtain, formally requiring expensive vertex corrections[3]. Other methods to calculate spectra of correlated extended systems, such as the dynamical density matrix renormalization group[12] or perturbative methods[13] are restricted to certain correlation strengths, system sizes or spatial dimensions.

Here, we bypass these issues, by extending the idea of quantum embedding of *states* rather than Greens func-

*Electronic address: ghb24@cam.ac.uk

tions, to compute dynamical correlation functions. The framework, which we term density matrix embedding theory (DMET) was introduced in Ref. 14, and extended to long-range Hamiltonians in Ref. 15. The essential idea for static quantities is that the Schmidt decomposition of a mean-field bulk state defines a *finite* quantum impurity mapping: for a cluster of l impurity sites there are l bath sites. The mapping is exact in the non-interacting and local limits, similar to DMFT, but has no bath discretization error, and because it is finite, is orders of magnitude cheaper numerically. Furthermore, the accuracy of DMET compares very favorably (and often exceeds) that of DMFT.

Here, we show that for dynamic quantities, the Schmidt decomposition of a mean-field bulk response vector yields a similar finite quantum impurity mapping that renders *spectra* exact in the non-interacting and local excitation limits. This 'spectral DMET' possesses significant advantages compared to DMFT. The finite quantum impurity mapping results in numerically simple calculations of spectral functions (no frequency point in these results took more than a minute on a single computing core), while eliminating bath discretization error of finite DMFT calculations. In addition, since the method is formulated in terms of a general response vector, it is not restricted in the type or rank of perturbation operators that it can consider, with two-particle Greens functions almost as easy to obtain as single particle Greens functions. The approach will be demonstrated for the Hubbard model, defined by the Hamiltonian in the site basis as

$$H = -t \sum_{\langle ij \rangle, \sigma} (a^\dagger_{i,\sigma} a_{j,\sigma} + \text{h.c.}) + U \sum_i (n_{i,\uparrow} - \frac{1}{2})(n_{i,\downarrow} - \frac{1}{2}). \tag{2}$$

This model encapsulates many of the challenges in the electronic structure of correlated materials, displaying correlation driven phase transitions in the thermodynamic limit, and the physics of many transition metal oxides[16], including qualitative features of high-T_c superconductivity[4, 5, 17]. Where possible, we compare to one-dimensional exact results from the Bethe Ansatz[18, 19], as well as large-scale 1D and 2D DMFT calculations at half-filling and under doping[20–22]. In addition we compute local two-particle Greens functions.

Method.- We first recap the DMET quantum embedding formalism introduced for the ground state, with more details provided in Ref. 14 and 15. The quantum impurity model and bulk properties are defined in the following steps. *i*) From the ground state of a one-particle Hamiltonian defined over the lattice, h, a single Slater determinant, $|\phi^{(0)}\rangle$, is variationally minimized. *ii*) A set of local 'impurity' sites are chosen, spanned by the states $\{|\alpha\rangle\}$, and the formal Schmidt decomposition of $|\phi^{(0)}\rangle = \sum_{\alpha\beta} \phi_{\alpha\beta} |\alpha\rangle|\beta\rangle$ into this space yields a set of bath states, $\{|\beta\rangle\}$, whose fock space is the same dimension as the impurity space. *iii*) The interacting quantum impurity plus bath Hamiltonian is constructed by projecting H into this basis of $\{|\alpha\rangle\} \otimes \{|\beta\rangle\}$ as $H' = PH_{emb}P$, with $P = \sum_{\alpha\beta} |\alpha\beta\rangle\langle\alpha\beta|$. This space spans the exact entanglement of the impurity to its environment within $|\phi^{(0)}\rangle$, and is now independent of the total number of sites in the system. To avoid double counting of correlation effects, H_{emb} is defined as the exact H over the impurity, while the one-particle h' is used over the rest of the space. *iv*) $H'|\Psi^{(0)}\rangle = E_0|\Psi^{(0)}\rangle$ is solved for the wavefunction over the quantum impurity and bath, $|\Psi^{(0)}\rangle$. *v*) A one-particle potential defined over the impurity space, u, is obtained in order to match the elements of the one-body density matrix of $|\phi^{(0)}\rangle$ and $|\Psi^{(0)}\rangle$. *vi*) This defines the new one-particle lattice Hamiltonian, $h' = h + u$ (where u is periodically repeated across the lattice), from which the process can be repeated until self-consistency. *vii*) Static, local expectation values are defined as $\langle\Psi^{(0)}|\hat{O}|\Psi^{(0)}\rangle$, while non-local expectation values, such as the energy, are defined in Ref. 14.

We now generalize to dynamic quantities. This requires the construction of a set of frequency-dependent bath states, into which the interacting dynamic response equations are projected. This procedure exactly embeds the local spectrum in the response of the entire (infinite) lattice, as defined by a response vector, $|\phi^{(1)}(\omega)\rangle$ constructed from the one-particle Hamiltonian, h'. *i*) The one-particle response vector is obtained from the solution to

$$\begin{aligned} |\phi^{(1)}(\omega)\rangle &= \left[\omega - (h' - \varepsilon_0) + i\eta\right]^{-1} \hat{V}|\phi^{(0)}\rangle \\ &= \hat{R}(\omega) \sum_{\alpha\beta} \phi^{(0)}_{\alpha\beta} |\alpha\rangle|\beta\rangle, \end{aligned} \tag{3}$$

where $\hat{R}(\omega)$ is the response operator relating $|\phi^{(0)}\rangle$ and $|\phi^{(1)}(\omega)\rangle$. For the one-particle Greens function, where $\hat{V} = a^{(\dagger)}_\alpha$, $\hat{R}(\omega) = \sum_i r_i(\omega) a^{(\dagger)}_i$, while for the two-particle Greens function, where $\hat{V} = a^{(\dagger)}_\alpha a^{(\dagger)}_{\alpha'}$, $\hat{R}(\omega) = \sum_{ij} r_{ij}(\omega) a^{(\dagger)}_i a^{(\dagger)}_j$. *ii*) The *operator* $R(\omega)$ is decomposed into separate operators as $R(\omega) = \sum_i \hat{\mathcal{A}}^{(i)}(\omega)\hat{\mathcal{B}}^{(i)}(\omega)$, where $\hat{\mathcal{A}}^{(i)}(\omega)$ act only on the local impurity states $\{|\alpha\rangle\}$, and $\hat{\mathcal{B}}^{(i)}(\omega)$ on the states of $\{|\beta\rangle\}$. *iii*) The Schmidt decomposition of $|\phi^{(1)}(\omega)\rangle$ takes the form

$$|\phi^{(1)}(\omega)\rangle = \sum_{\alpha\beta i} \phi^{(0)}_{\alpha\beta} |\alpha\rangle \hat{\mathcal{B}}^{(i)}|\beta\rangle. \tag{4}$$

$|\phi^{(1)}(\omega)\rangle$ lives in the space $\mathcal{K}(\omega) = \{|\alpha\rangle\} \otimes \{\hat{\mathcal{B}}^{(i)}(\omega)|\beta\rangle\}$ which then defines the projector $P(\omega) = |\mathcal{K}(\omega)\rangle\langle\mathcal{K}(\omega)|$, into which the interacting response equations are projected. *iv*) The interacting response vector, $|\Psi^{(1)}(\omega)\rangle$, is calculated from

$$P\left[\omega - (H_{emb} - E_0) + i\eta\right] P|\Psi^{(1)}(\omega)\rangle = P\hat{V}P|\Psi^{(0)}\rangle, \tag{5}$$

which in this work is solved via an exact, iterative procedure[23]. $|\Psi^{(0)}\rangle$ can be reoptimized in the larger space of $\mathcal{K}(\omega)$, however this was found not to qualitatively change the results, and so $|\Psi^{(0)}\rangle$ and E_0 are taken to be the ground-state wavefunction and energy in the original quantum impurity and bath space of $\{|\alpha\rangle\} \otimes \{|\beta\rangle\}$. *v*) The final spectral function is obtained as $G(\omega; \hat{X}, \hat{V}) = \langle\Psi^{(0)}|P\hat{X}^\dagger P|\Psi^{(1)}(\omega)\rangle$.

There are a number of points to note about the above construction. For simplicity, we restrict ourselves here to consider *local* spectral functions, where $\hat{V}$ and $\hat{X}$ are both closed operators within the space of $\{|\alpha\rangle\}$, although extensions to non-local perturbations will be detailed in a forthcoming paper. The set of operators $\hat{\mathcal{B}}^{(i)}(\omega)$ include the unit operator. This ensures that the space of

the ground-state DMET is included within $\mathcal{K}(\omega)$. The rest of the $\hat{\mathcal{B}}^{(i)}(\omega)$ operators define frequency-dependent bath states, which may not always be orthogonal, but nonetheless exactly 'span' $|\phi^{(1)}(\omega)\rangle$ throughout the lattice. This ensures that the spectral functions are exact in the $U = 0$ non-interacting limit, where h', and therefore $|\phi^{(1)}(\omega)\rangle$ are also exact. Away from this limit, $|\phi^{(1)}(\omega)\rangle$ also changes, due to the presence of the interaction potential u in the one-particle Hamiltonian, which includes local interaction effects of the system. In addition, $|\Psi^{(1)}\rangle$ is also exact for uncoupled, local excitations within the impurity cluster, due to the completeness of the impurity space $\{|\alpha\rangle\}$ included in $\mathcal{K}(\omega)$. Finally, we note that although the above bath construction was carried out at zero temperature, a similar finite temperature construction exists by carrying out decompositions in the super-operator space.

The exactness of the non-interacting and local limits is a feature that this construction shares with DMFT, but there are important properties which DMFT does not posess. The coupling to the environment is achieved via a set of bath states, which change continuously with frequency, and which couple the impurity space to the set of non-local excitations appropriate for the frequency considered. In contrast, DMFT constructs bath states which are frequency-independent, and whose size must be formally infinite in order to avoid a discretization error which is not present in the above *algebraic* construction. Furthermore, DMFT is formulated in terms of the one-particle Greens function, but the procedure outlined above is suitable for general operators $\hat{V}$ of any rank. A key point of the approach is that the analytic construction of the bath states which exactly span $|\phi^{(1)}(\omega)\rangle$, is no more costly than the diagonalization of the one-particle Hamiltonian, h, and once the fully interacting response is projected into this basis, there is no dependence on the size of the underlying lattice, rendering the cost of the method truly mean-field scaling with the size of the system[25].

It is now necessary to turn to numerical applications of the method to determine the quality of the results away from these exact limits. In this Letter, we restrict ourselves to consider the one- and two-particle local Greens functions, defining the local density of states, and density-density spectral functions respectively, while other local dynamic correlation functions can be obtained analogously.

Results.- We first examine the one-dimensional Hubbard model, whose ground state energy[18] and spectral gap[19] are obtainable from the Bethe-Ansatz, and additionally compare to zero-temperature, cluster-DMFT results[20]. Figure 1 shows the local density of states, calculated with a four-site DMET impurity cluster, and compared to six-site cluster-DMFT results, obtained via an exact diagonalization within six bath orbital representation, as described in Ref. 20. Both DMET and DMFT calculation are performed in the paramagnetic phase. Since exact diagonalization was used as the impurity solver, the spectra are obtained on the real axis at zero-temperature, and so can be directly compared against. As expected in the one-dimensional case, there is no frustration, and the system is dominated at all values of U by long-range magnetic ordering[18]. Consequently,

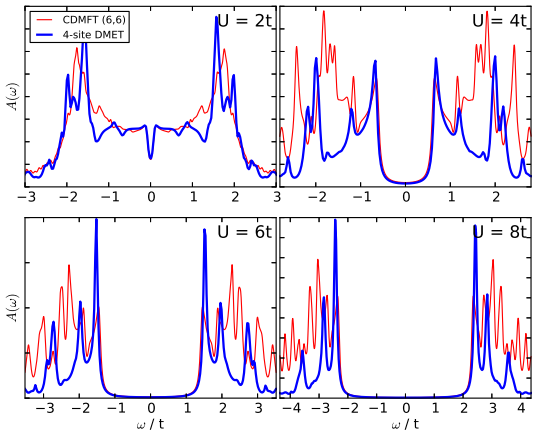

FIG. 1: Comparison of the local density of states between a four impurity cluster DMET calculation and a (six impurity, six bath) CDMFT calculation for the half-filled 1D Hubbard model. The analytic bath construction of DMET renders the spectral functions smooth over the frequency range, with the same spectral broadening ($\eta = 0.05t$) used for both the CDMFT and DMET calculations.

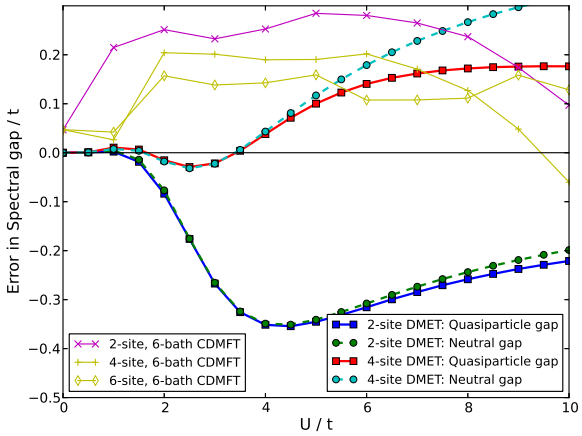

FIG. 2: Error in the spectral gap from the 1-particle and 2-particle Greens functions compared to analytic results from the Bethe Ansatze[19], and six bath orbital CDMFT results[20]. The results show generally good agreement between the Greens functions, and convergence of the DMET results with increasing cluster size.

the system is insulating for arbitrarily small values of U, in both the DMET and CDMFT spectra.

The spectral gaps are very similar in the DMET and CDMFT calculations, however, the higher frequency excitations in the CDMFT calculations are very noisy, which makes it difficult to determine which features are physical, and which are spurious and a result of the finite (six) bath representation of the coupling of the cluster to the environment. In contrast, the DMET results give an entirely smooth representation of the spectra, due to the analytic construction of the exact coupling to $|\phi^{(1)}(\omega)\rangle$ at each frequency. However, at very high frequencies, outside the bandwidth of $|\phi^{(1)}(\omega)\rangle$, there is no coupling of the local excitations to the environment provided by the DMET bath construction and so uncoupled local excitations result. Therefore, in the results presented, the spectral window probed will be determined by the band-

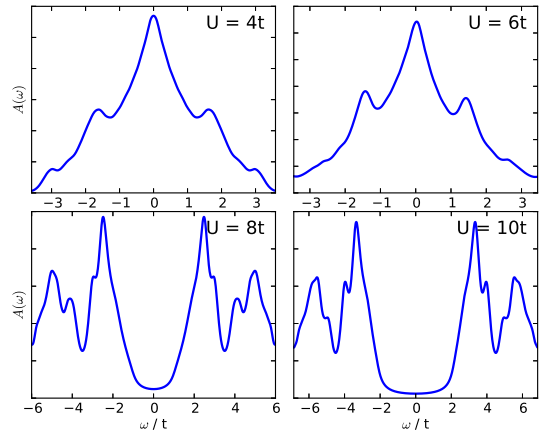

FIG. 3: Local density of states of the half-filled 2D Hubbard model from a 2×2 impurity cluster DMET calculation, with a MIT at $U \approx 6.9t$. The exact bath states from $|\phi^{(1)}(\omega)\rangle$ for each frequency allows for smooth spectral functions at real frequencies.

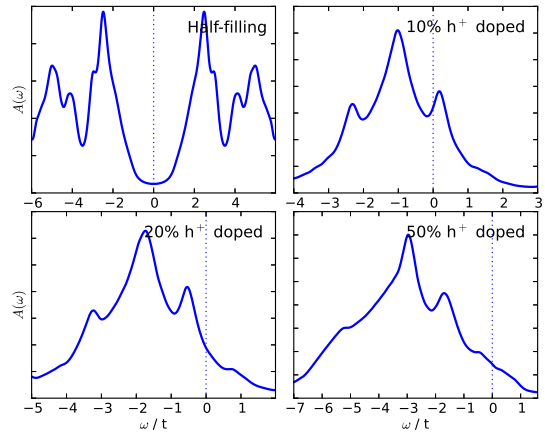

FIG. 4: Local density of states of the hole doped 2D Hubbard model calculated with a 2×2 impurity cluster with $U = 8t$. Qualitative features present in the CDMFT study of Ref. 22 are observed (see Fig. 1(c) and (d)).

width of $|\phi^{(1)}(\omega)\rangle$. Another point to note is that the sum rules on the spectral functions are exactly obeyed, and the integrated spectral weight of the results in Fig. 1 are all unity. For comparison, Fig. 2 shows the error in the spectral gap from the exact Bethe Ansatz result[19], demonstrating the convergence towards the exact spectral gap as the cluster size is increased from two to four sites, and indicating a generally similar quality to CDMFT calculations of similar cluster size.

A sterner test comes from the 2D Hubbard model. Cluster DMFT calculations in the paramagnetic phase exhibit a metal-insulator transition (MIT) at finite U, representative of a Mott transition[3, 5, 7, 10, 13, 21]. The DMET local density of states are shown in Fig. 3 for a 2×2 plaquette of impurity sites. In the low U regime, the famous 'three-peak' structure is observed, with a central Kondo resonance peak, and the Hubbard bands either side. At $U \approx 6.9t$, there is a transition to an insulating regime, with a Mott gap opening with increased U. The spectra then feature prominent coherence peaks at the gap edge, as have been observed elsewhere[21]. Cluster

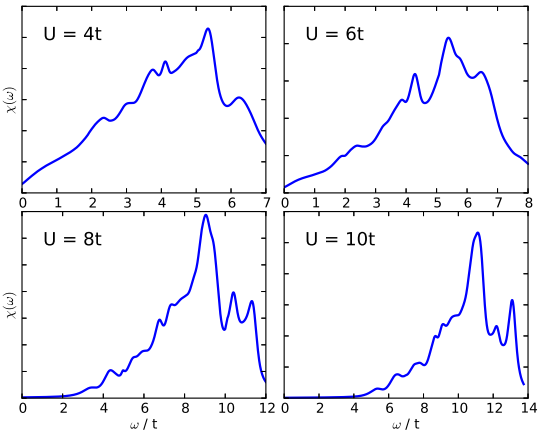

FIG. 5: 2×2 impurity DMET calculation of the local density-density response function for the half-filled 2D Hubbard model.

DMFT calculations with the same plaquette size observe a MIT at a slightly lower $U \approx 5.5t$, with a coexistence region at low temperatures, which we also observe. However, analytically continued spectral functions from CT-QMC smooth out many of the subtle correlation driven substructures observed in Fig. 3. Fig. 4 shows the effect on the spectra upon hole doping the system, which is shown for the insulating phase at $U = 8t$. Once doped, the weight is transferred to lower frequencies until the system becomes a Fermi liquid phase. The spectra are qualitatively similar to those seen in recent cluster DMFT studies[22].

Fig. 5 shows the local density-density response function of the 2D Hubbard model at half-filling, obtained from the local two-particle Greens function ($\hat{V} = \hat{X} = a^\dagger_{\alpha_\alpha} a_{\alpha_\alpha} + a^\dagger_{\alpha_\beta} a_{\alpha_\beta}$). The poles of this function correspond to the neutral excitation energies, and as such determine the optical properties of the system[3, 24]. Unfortunately, direct comparison of the spectra in Fig. 5 to other results is difficult due to the paucity of other comparable calculations for this quantity, but show the expected MIT, and transfer of spectral weight to higher frequencies as U increases. However, since holons and doublons do not bind in the 1D Hubbard Hamiltonian, the optical and single-particle gaps obtained should be the same, and these can be tested against the exact Bethe Ansatz results as before[24]. Therefore, excitation gaps obtained from the two-particle Greens functions in the 1D model are included in Fig. 2, and show that for the same cluster size, the differences between the spectral gaps are generally small. While not conclusive, this supports the assertion that the one- and two-particle Greens functions are of similar quality, while also of comparable computational cost, and validating the results shown in Fig. 5.

In conclusion, we have presented a quantum embedding formalism for accurate, zero-temperature spectral functions of extended, strongly correlated systems at a small computational cost, which vastly extends the scope of the DMET method. The approach has a number of advantageous formal properties. *i*) The embedding within the environment is achieved via coupling to a small set of analytically constructed, many-particle bath states, which are derived from the formal Schmidt decomposition of

the response vector obtained from a one-particle Hamiltonian. The quantum impurity plus bath space therefore exactly spans this vector, and changes with frequency, to give smooth spectra without any error from the discretization of the continuum. *ii*) The simple finite size quantum impurity model allows spectral functions to be easily obtained on the real frequency axis, removing the need for any analytic continuation from the imaginary axis. *iii*) The interacting quantum impurity and bath space is independent of the size of the underlying lattice, and is constructed at a cost no greater than the diagonalization of the one-particle Hamiltonian *iv*) Both extension to clusters of impurity sites, and arbitrary dynamic correlation functions are straightforward within the framework. The approach was demonstrated on the one- and two-dimensional Hubbard model, and compared favorably to both exact results and cluster DMFT calculations. Extensions are now underway for the calculation of non-local operators, an *ab initio* formulation, and for the investigation of differently ordered phases by embedding within broken symmetry mean-field Hamiltonians.

Acknowledgements

The authors would like to sincerly thank Ara Go for sharing her CDMFT results and useful conversations.

[1] J. E. Coulter, E. Manousakis, and A. Gali (2013), arXiv:1306.4948.
[2] A. Mukherjee, G. A. Sawatzky, and M. Berciu, Phys. Rev. B **87**, 165136 (2013).
[3] N. Lin, E. Gull, and A. J. Millis, Phys. Rev. Lett. **109**, 106401 (2012).
[4] G. Sordi, P. Sémon, K. Haule, and A.-M. S. Tremblay, Phys. Rev. Lett. **108**, 216401 (2012).
[5] E. Gull, O. Parcollet, and A. J. Millis, Phys. Rev. Lett. **110**, 216405 (2013).
[6] A. Georges and W. Krauth, Phys. Rev. Lett. **69**, 1240 (1992).
[7] A. Georges, G. Kotliar, W. Krauth, and M. Rozenberg, Rev. Mod. Phys. **68**, 13 (1996).
[8] G. Kotliar, S. Y. Savrasov, K. Haule, V. S. Oudovenko, O. Parcollet, and C. A. Marianetti, Rev. Mod. Phys. **78**, 865 (2006).
[9] P. Werner, A. Comanac, L. de' Medici, M. Troyer, and A. J. Millis, Phys. Rev. Lett. **97**, 076405 (2006).
[10] D. Zgid, E. Gull, and G. K.-L. Chan, Phys. Rev. B **86**, 165128 (2012).
[11] S. Fuchs, E. Gull, M. Troyer, M. Jarrell, and T. Pruschke, Phys. Rev. B **83**, 235113 (2011).
[12] H. Benthien, F. Gebhard, and E. Jeckelmann, Phys. Rev. Lett. **92**, 256401 (2004).
[13] D. Senechal, D. Perez, and M. Pioro-Ladiere, Phys. Rev. Lett. **84**, 522 (2000).
[14] G. Knizia and G. K.-L. Chan, Phys. Rev. Lett. **109**, 186404 (2012).
[15] G. Knizia and G. K.-L. Chan, J. Chem. Theory Comput. **9**, 1428 (2013).
[16] P. Limelette, A. Georges, D. Jerome, P. Wzietek, P. Metcalf, and J. Honig, Science **302**, 89 (2003).
[17] P. W. Anderson, Science **235**, 1196 (1987).
[18] E. Lieb and F. Wu, Phys. Rev. Lett. **20**, 1445 (1968).
[19] A. Ovchinni, Sov. Phys. JETP-USSR **30**, 1160 (1970).
[20] A. Go and G. S. Jeon, J. Phys.: Condens. Mat. **21**, 485602 (2009).
[21] H. Park, K. Haule, and G. Kotliar, Phys. Rev. Lett. **101**, 186403 (2008).
[22] S. Sakai, Y. Motome, and M. Imada, Phys. Rev. Lett. **102**, 056404 (2009).
[23] V. Fraysse, L. Giraud, S. Gratton, and J. Langou, ACM T. Math. Software **31**, 228 (2005).
[24] F. Essler, V. Korepin, and K. Schoutens, Phys. Rev. Lett. **67**, 3848 (1991).
[25] A pilot implementation used to obtain these results can be found at https://github.com/ghb24/SpectralDMET.git